Cement & Concrete Composites 30 (2008) 706–714

Contents lists available at ScienceDirect

Cement & Concrete Composites

journal homepage: www.elsevier.com/locate/cemconcomp

Microstructures of reactive magnesia cement blends

L.J. Vandeperre *, M. Liska, A. Al-Tabbaa

Department of Engineering, University of Cambridge, Trumpington Street, Cambridge CB2 1PZ, UK

ARTICLE INFO

Article history:
Received 5 June 2006
Received in revised form 27 March 2008
Accepted 8 May 2008
Available online 15 May 2008

Keywords:
Microstructure
Hydration products
Reactive magnesia cement

ABSTRACT

The microstructures of reactive magnesia cement blends, consisting of mixtures of a reactive magnesium oxide (MgO), Portland cement (PC) and pulverised fuel ash (pfa), as observed with scanning electron microscopy are reported. To allow identification of the hydration products of MgO, mixtures of pfa and MgO only were also studied and mixtures of PC and pfa were included as a reference point for comparison. Mixtures with 90 wt% pfa, were found to have a microstructure, which consists of weakly bonded spheres stacked together; when the pfa content is reduced to 50 wt%, the microstructure changes to spheres packed into a solid matrix. For mixtures with a high MgO content, up to 50 wt%, however, the microstructures remain more open and particulate in nature due to the high water demand of reactive MgO. It is shown that these changes in microstructure are consistent with a simple estimate based on the volume fraction of solids formed during hydration. X-ray diffraction studies confirmed that in these blends MgO reacts mainly with water to form magnesium hydroxide, with hydrotalcite as a minor reaction product, and that for the reactive MgO used here hydration completes early on so that there should be no risk for damage due to later-age hydration. Moreover, comparison of X-ray diffraction patterns obtained from mixtures containing either PC and pfa or MgO and pfa with those of blends containing PC, MgO and pfa, shows little evidence of interaction between PC and MgO in terms of the hydration products that are formed.

1. Introduction

Reactive magnesia cements is a new group of cements based on magnesium oxide (MgO) that were proposed 5 years ago [1] and which consist of mixtures of a reactive MgO powder blended with a hydraulic cement and also a pozzolan. The use of MgO in cements is not new: MgO has been used for example in *Sorel* cements and in magnesium phosphate cements. The setting in the former is based on the reaction between $MgCl_2$ and MgO, which results in the formation of various oxychlorides [2–4], while in magnesium phosphate cements, MgO is reacted with a soluble phosphate forming magnesium phosphates [5–7]. In contrast, in reactive MgO cements, it is claimed that the MgO contributes to the strengthening of the cement by reacting with water to form magnesium hydroxide ($Mg(OH)_2$ or brucite) [1]. As the volume expansion due to the hydration of MgO has been linked with damage, normal practice is to limit the quantity of MgO that can be present in e.g. Portland cement to typically less than 1% [5]. However, such cracking occurs only when the expansion of the material is constrained, which arises when the hydration of MgO occurs much later than that of the major cement phases. It was claimed that if a sufficiently reactive MgO is used, the hydration would occur at a sufficient rate not to cause any problems due to late hydration [1], and that this can be achieved by calcining at lower temperatures (<750 °C) [1] so that the material retains a high surface area. However, these claims have so far not been substantiated.

The aim of this paper therefore was to investigate the types of microstructures that form when reactive MgO, pulverised fuel ash (pfa) and Portland cement (PC) are blended and to confirm that a reactive MgO hydrates almost completely at an early enough stage so that expansion related problems can be avoided. To enable a better identification of the hydration products due to MgO and to study whether there is any evidence of an interaction between PC and MgO, mixtures containing only MgO and pfa were studied alongside mixtures containing PC, MgO and pfa. To allow a comparison to be made with the microstructures obtained without MgO, mixtures with PC and pfa alone were also studied.

2. Materials and experimental methods

The materials used in the blends were reactive magnesium oxide (MgO), pulverised fuel ash (pfa), and Portland cement (PC). The same MgO source was used as in the original work [1], and this material is commercially available (Grade XLM, Causmag International, Young, Australia), the pfa was a run-of station pfa obtained directly from a power station (Powergen, Ratcliffe on Soar, UK), and

* Corresponding author. Present address: Department of Materials, Imperial College London, London SW7 2AZ, UK. Tel.: +44 0207 594 6766; fax: +44 0207 594 6757.
E-mail address: l.vandeperre@imperial.ac.uk (L.J. Vandeperre).

0958-9465/$ - see front matter © 2008 Elsevier Ltd. All rights reserved.
doi:10.1016/j.cemconcomp.2008.05.002

the Portland cement was a CEM-I (Blue Circle CEM-I, Lafarge, Oxon, UK). The chemical composition was measured with an electron probe microanalysis system attached to an SEM and is reported in Table 1 together with the specific surface area as measured by nitrogen adsorption (BET).

The compositions of the blends studied are reported in Table 2 together with an abbreviated notation that will be used throughout the paper. There are two groups of compositions, which differ by their pfa content. In the first group the weight fraction of pfa amounted to 0.9, while in the second group the amount of pfa was reduced to a weight fraction of 0.5. Both groups contained mixes with either PC alone or MgO alone as well as mixes where MgO and PC were used together.

Mixes of typically 3–3.5 kg material were prepared with the aid of a laboratory bench top mixer by first adding all water and then incrementally adding the dry material to the mix. To ensure a homogeneous distribution of the different solids these were dry mixed before they were added to the water. Occasionally, the mixer was stopped to mix in that part of the paste, which collected above the main mix on the sides of the mixing bowl. The water to solids ratio (w/s) was initially fixed at 0.4 for all compositions studied. However, for two compositions a homogeneous paste could not be made at this water content, and the water content was therefore increased as detailed in Table 2. To confirm this observation in a more objective manner, the standard consistence of the pastes was measured according to BS EN 196-3:1995 [8], and the results, also reported in Table 2, confirmed that pastes with a higher MgO content do require a higher water to solids ratio for the same consistence.

Following mixing, samples were prepared by placing the paste into cylindrical moulds (Ø50 × 100 mm). Care was taken to reduce the amount of air voids as much as was practically possible. The samples were then cured in containers at a relative humidity of 98%.

The microstructure was studied by imaging fracture surfaces in a scanning electron microscope (SEM, JEOL 820, Japan). Identification of the crystalline phases present was performed by X-ray diffraction using Cu Kα radiation (PW1050, Philips, Eindhoven, The Netherlands).

Table 1
Chemical composition, specific surface area (BET) of the raw materials

	MgO	pfa	PC
	Causmag XLM	Ratcliffe on Soar power station	Lafarge blue circle
CaO	1.2	4.4	63.6
SiO_2	1.2	43.6	13.9
Fe_2O_3	0.2	14	2.7
Al_2O_3	0.2	26	10.2
MgO	97.2	4	0.6
K_2O	(–)	3.5	0.9
Na_2O	(–)	0.9	(–)
TiO_2	(–)	1.5	0.1
SO_3	(–)	1.7	6.9
SSA	75.2	3.43	1.5

3. Results

Fig. 1 shows representative micrographs of the raw materials. The MgO powder in Fig. 1a consists of fine particles, which appears to have agglomerated into larger groups of particles. The pfa is shown in Fig. 1b and consists mostly of spherical particles of varying size, and the PC powder, see Fig. 1c, is angular, which is consistent with the shape of powder particles produced by grinding. The X-ray diffraction patterns of the starting materials are shown in Fig. 2. The diffraction pattern of the pfa shows a broad peak, which

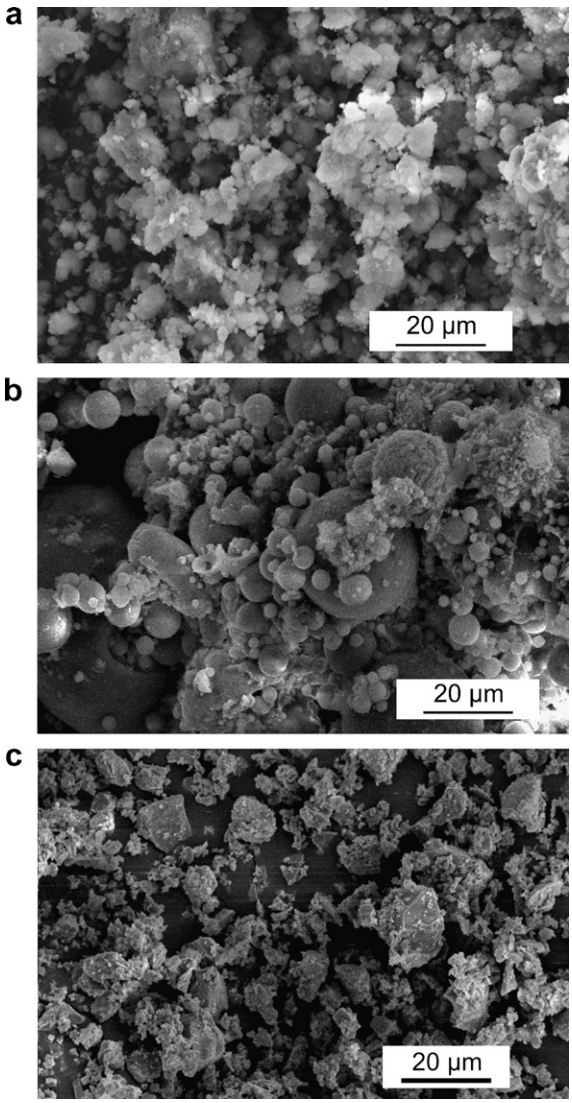

Fig. 1. Secondary electron micrographs of the raw materials used: (a) reactive MgO, (b) pfa and (c) Portland cement.

Table 2
Composition of the blends, water to solids ratio (w/s) the water to solids ratio for standard consistence $(w/s)_{SC}$, and the volume fraction of solids in the blends, $(1 - P)$

Reference	pfa (wt%)	MgO (wt%)	PC (wt%)	w/s	$(w/s)_{SC}$	$(1 - P)$
$MgO_{0.1}$–$pfa_{0.9}$	90	10	0	0.40	0.390	0.54
$(MgO_{0.8}PC_{0.2})_{0.1}$–$pfa_{0.9}$	90	8	2	0.40	0.390	0.54
$(MgO_{0.5}PC_{0.5})_{0.1}$–$pfa_{0.9}$	90	5	5	0.40	0.385	0.54
$PC_{0.1}$–$pfa_{0.9}$	90	0	10	0.40	0.37	0.54
$MgO_{0.5}$–$pfa_{0.5}$	50	50	0	0.60	0.53	0.39
$(MgO_{0.8}PC_{0.2})_{0.5}$–$pfa_{0.5}$	50	40	10	0.43	0.465	0.48
$(MgO_{0.5}PC_{0.5})_{0.5}$–$pfa_{0.5}$	50	25	25	0.40	0.405	0.50
$PC_{0.5}$–$pfa_{0.5}$	50	0	50	0.40	0.323	0.50

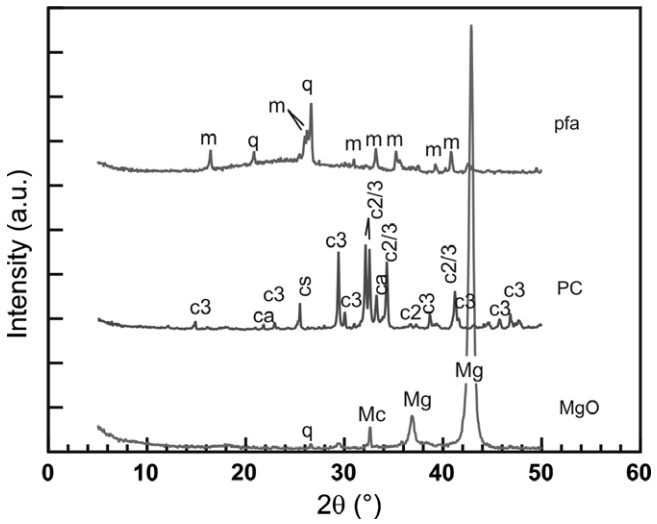

Fig. 2. X-ray diffraction patterns of the raw materials. Only the major phases have been indicated: q: quartz, m: mullite, ca: calcium aluminate, c3: tri-calcium silicate, c2: di-calcium silicate, cs: calcium sulphate, Mg: magnesium oxide, Mc: magnesium carbonate.

extends between 15° and 35°2θ and which is due to the presence of amorphous or glassy material. There is also crystalline material with quartz and mullite being the major phases. This is consistent with what has been observed elsewhere [9]. In the pattern for the cement, the normal phases such as di-calcium silicate, tri-calcium silicate and aluminium silicate expected in a CEM-I [10] are found. The magnesium oxide powder contains a small amount of quartz consistent with the results of the chemical composition, and a small amount of magnesium carbonate.

Fig. 3 shows low magnification scanning electron micrographs of fracture surfaces of all types of samples at 14 days. For samples containing a weight fraction pfa of 0.9, the replacement of PC by MgO has little influence on the overall microstructure, see Fig. 3a–d, which at this magnification resembles a stack of spherical pfa particles, as can be seen by comparing the microstructures with Fig. 1b.

For samples containing a weight fraction pfa of only 0.5 Fig. 3e through to 3 h illustrate that when MgO replaces PC the change in microstructure is sufficient for it to be noticeable even at relatively low magnification. For a sample containing only MgO and pfa, Fig. 3e, the particulate nature of the microstructure also observed for the high pfa contents is retained, although the fraction of fine particles has clearly increased. These finer particles are very similar in size and shape to the original MgO powder, see Fig. 1a, and hence at low magnification the difference in the microstructure with samples containing much more pfa is due to the shape and size of the particles, which are packed together. However, as the amount of PC is increased, as in Fig. 3f–h, quite a different microstructure forms: the pfa particles remain visible but appear to be covered up by a continuous matrix into which they are embedded.

3.1. Details of microstructures containing only MgO and pfa

As shown in Fig. 4a and b, closer inspection of the microstructure of samples with a weight fraction pfa of 0.9, shows that the pfa particles have been covered in a pattern of very small particles. The extent of coverage is substantial but not enough material has formed to create a continuous film on the surface of the particles. Some of the pfa particles show regions where no hydration product is present as can be seen for example at point "**A**" in Fig. 4b. The shape of these regions strongly suggests that at these locations two pfa particles were in contact before the sample was fractured for observation in the microscope, which explains the absence of any deposition of hydration products. At much higher MgO content, and therefore a lower pfa content, as shown in Fig. 4c and d, the hydration products have formed a continuous film on the surface of the pfa particles, as can be seen at point "**C**" in Fig. 4c. In addition, there are now also regions where MgO particles are linked together by hydration products, as for example at point "**B**" in Fig. 4c. Closer observation, Fig. 4d, also shows that due to the abundance of the hydration products the appearance has changed from the small isolated dots found at low MgO content into a tangled web of flake-like crystals.

The X-ray diffraction pattern obtained at an age of 64 days, which is shown in Fig. 5, shows that hydration has resulted in the formation of magnesium hydroxide ($Mg(OH)_2$, Brucite) and a very small amount of hydrotalcite ($Mg_6Al_2(CO_3)(OH)_{16}(H_2O)_4$). The identification of the latter based on the X-ray diffraction pattern obtained at this age is very tentative, but in diffraction patterns of similar samples, which have been cycled through wet and dry twice a week for 180 days to enhance precipitation of material, this peak strengthens and secondary peaks become apparent so that identification becomes possible as also shown in Fig. 5. Moreover, the formation of brucite and hydrotalcite is consistent with results by Ghanbari et al. [11,12], who on the basis of X-ray diffraction data reported the formation of brucite and hydrotalcite when MgO and alumina (Al_2O_3) were mixed in a weight ratio of 2 to 1. In experiments by the same authors, brucite was the major hydration product when MgO hydrates alone or in the presence of fumed silica. In addition to brucite and hydrotalcite, the formation of magnesium silicate hydrate (M–S–H) is in principle possible due to the silica present in the pfa. M–S–H gels are known to form in aqueous solutions containing Mg^{2+} and SiO_3^{2-} ions [13] and hydrated magnesium silicates have been reported in the breakdown of a concrete sea-wall [14] and in magnesium sulphate attack of cement [15]. However, M–S–H gels are poorly crystalline and hence give broad X-ray diffraction peaks, which are difficult to discern against the broad background due to the pfa. As a simple method to better establish whether there is any evidence for M–S–H formation here, the diffraction signal due to pfa was removed from the diffraction patterns shown in Fig. 5 by subtracting half the intensities recorded for pfa alone. The so obtained patterns are shown in Fig. 6. The deconvoluted diffraction pattern for $MgO_{0.5}$–$pfa_{0.5}$ has a flat background suggesting that if any M–S–H has formed, the amount is probably small.

The intensity of the peaks due to MgO has decreased substantially, confirming that this reactive MgO powder has hydrated almost completely in 64 days and therefore when a reactive MgO is used there should be little risk of disruptive late hydration.

3.2. Details of microstructures containing only PC and pfa

As shown in Fig. 7a and b, for samples with a weight fraction pfa of 0.9 and the remainder Portland cement, the pfa particles have been covered in hydration products, and the products form a more continuous layer compared to the coverage observed for MgO hydration. The hydration products consist of a mixture of phases as is typical for Portland cement, with for example Portlandite visible at point "**A**" in Fig. 7b, intermixed with reticulated C–S–H gel (point "**B**" in Fig. 7b). The reticulation suggests that the density of the C–S–H was relatively low so that upon vacuum drying before placing into the electron microscope much of the structure has collapsed leaving only the reticulated network behind. High magnification images of the microstructure of samples with a weight fraction pfa of 0.5, show that the matrix which completely engulfs the pfa particles is again a mixture of phases,

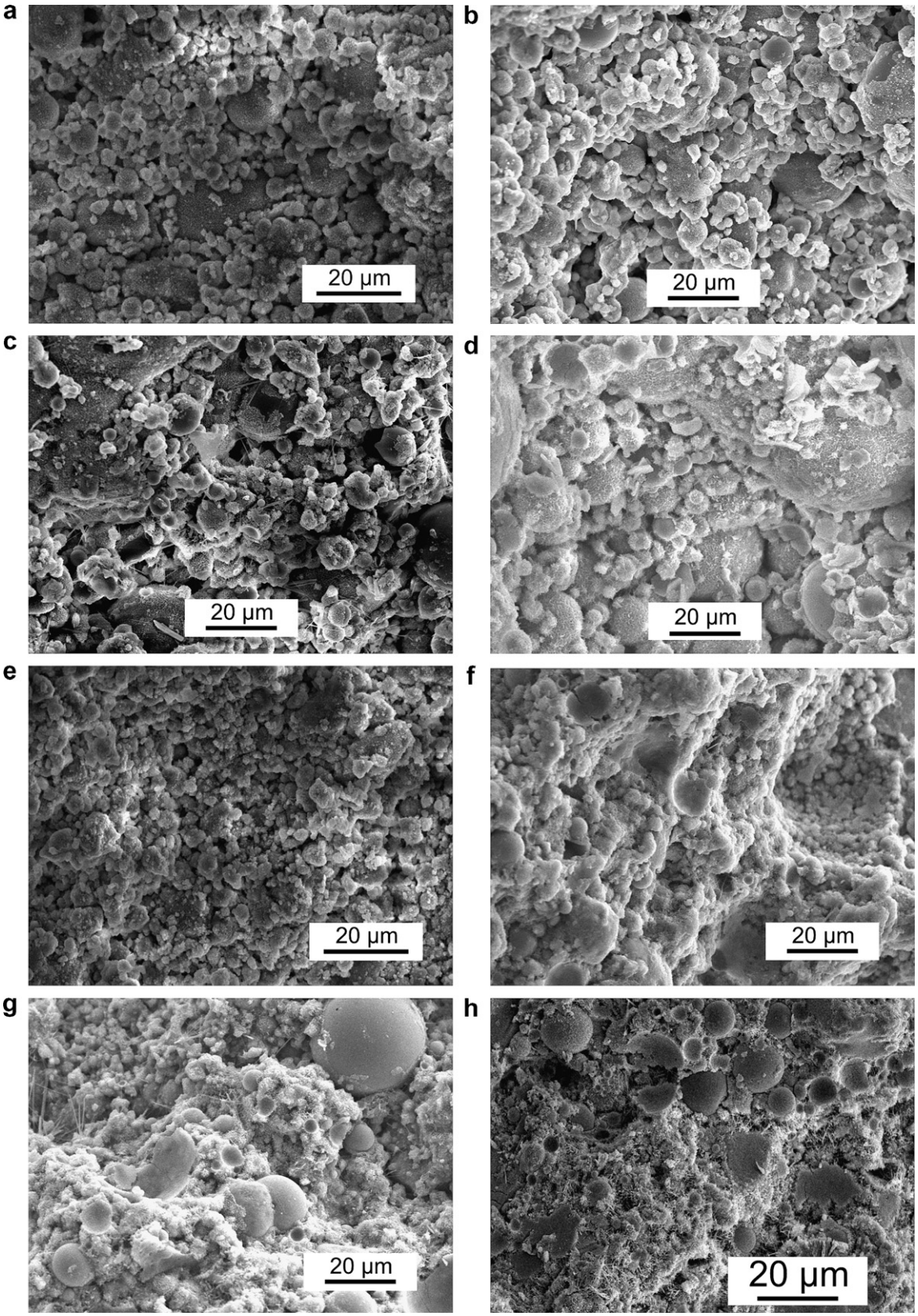

Fig. 3. Low magnification secondary electron micrographs after 14 days of curing of the 50% and 90% pfa content mixes: (a) $MgO_{0.1}$-$pfa_{0.9}$, (b) $(MgO_{0.8}PC_{0.2})_{0.1}$-$pfa_{0.9}$, (c) $(MgO_{0.5}PC_{0.5})_{0.1}$-$pfa_{0.9}$, (d) $PC_{0.1}$–$pfa_{0.9}$, (e) $MgO_{0.5}$–$pfa_{0.5}$, (f) $(MgO_{0.8}PC_{0.2})_{0.5}$-$pfa_{0.5}$, (g) $(MgO_{0.5}PC_{0.5})_{0.5}$-$pfa_{0.5}$ and (h) $PC_{0.5}$–$pfa_{0.5}$.

with some areas showing the reticulation, see e.g. point "D" in Fig. 7d, but in other areas and mostly where a layer has covered the pfa particles, a closer packing of hydration products appears to have formed, see e.g. point "C" in Fig. 7d. This is consistent with the concept that C–S–H gel forms in at least two variants, a low-density and a high density C–S–H [16–18], and with predic-

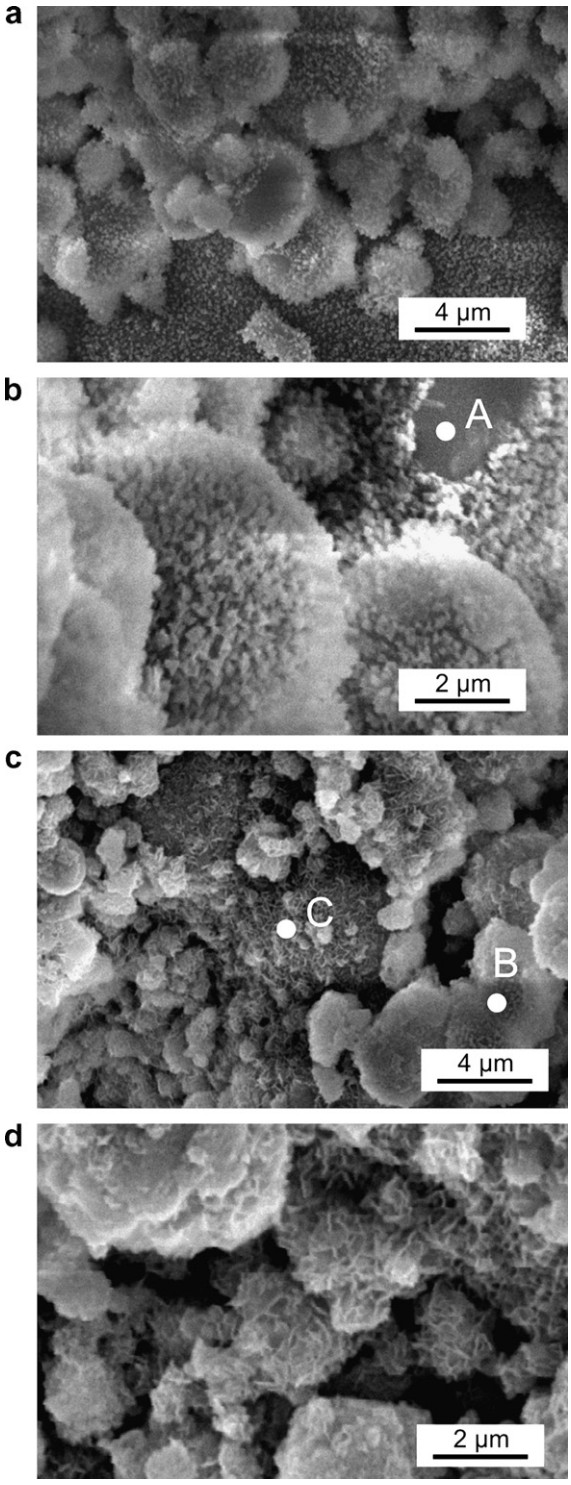

Fig. 4. High magnification secondary electron micrographs at 14 days of samples with compositions (a–b) $MgO_{0.1}$–$pfa_{0.9}$, (c–d) $MgO_{0.5}$-$pfa_{0.5}$.

tions and experimental data [17], which indicate that if more space is provided more of the low-density variant will form. X-ray diffraction confirmed the presence of typical crystalline hydration products such as Ettringite and Portlandite and some residual di-calcium silicate in addition to the phases due to the pfa, see Fig. 5. The presence of residual di-calcium silicate is not surprising as it is known that this clinker phase hydrates relatively slowly [5]. Against the broad background of the glassy material within the pfa, the presence of the relatively amorphous

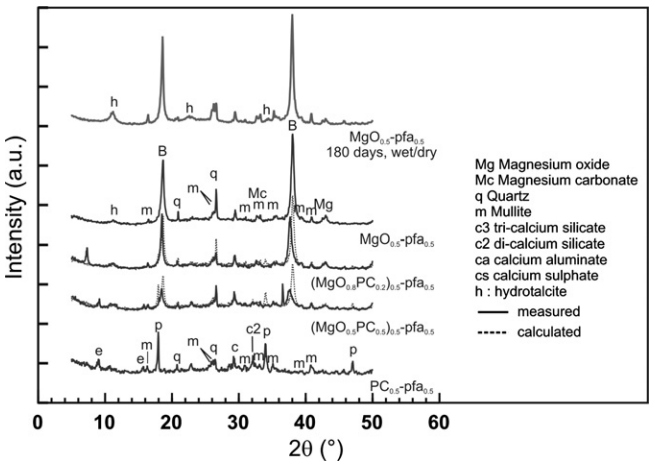

Fig. 5. X-ray diffraction patterns of samples cured for 64 days. The dashed lines on the two central diffraction patterns are a linear combination of the two diffraction patterns with only pfa and PC or only pfa and MgO. Also shown is a diffraction pattern obtained from a sample after it had been cycled between wet and dry two times per week for 180 days.

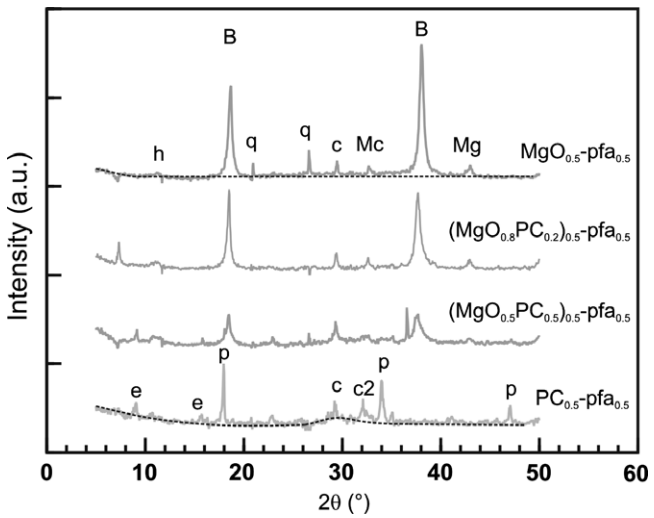

Fig. 6. The X-ray diffraction patterns shown in Fig. 4 after subtracting the intensity due to pfa (B: brucite, q: quartz, h: hydrotalcite, Mc: magnesium carbonate, Mg: magnesium oxide, p: Portlandite, e: ettringite, c: calcite, c2 di-calcium silicate).

C–S–H gel [5] is difficult to confirm, but after removal of the intensities due to pfa, as shown in Fig. 6, it becomes clear that there is indeed a broad peak in the background between 20° and 40°2θ consistent with the X-ray diffraction pattern of C–S–H gels [19].

3.3. Details of microstructures containing MgO, PC and pfa

Figs. 8 and 9 show details of the microstructures obtained when MgO, PC and pfa are all present in the blend. Needle-like features such as near point "**A**" in Fig. 8d become more abundant as the amount of PC is increased. These needles are probably Ettringite and their increased presence with increased PC concentration is consistent with the X-ray diffraction results, see Fig. 5, which show that Ettringite only forms in samples containing PC.

The microstructural observations suggest that when both MgO and PC are present in addition to pfa, the resulting microstructure is a simple mixture of the products obtained when either MgO and pfa or PC and pfa are combined. This is perhaps clearer in the

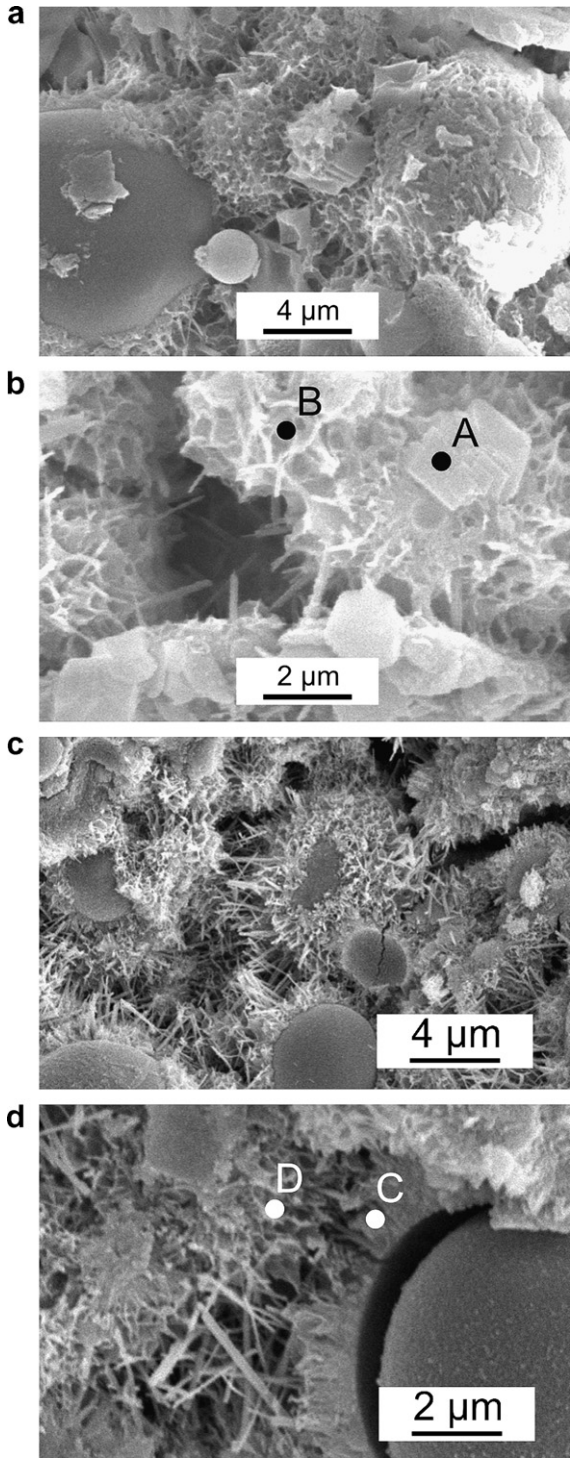

Fig. 7. Secondary electron micrographs after 14 days of hydration of samples with compositions (a–b) $PC_{0.1}$-$pfa_{0.9}$, (c–d) $PC_{0.5}$-$pfa_{0.5}$.

microstructures with 90 wt% pfa, which are shown in Fig. 8. For a MgO to PC ratio of 4 to 1, shown in Fig. 8a and b, the appearance of the hydration products on the pfa particles is still quite similar to what is observed in samples without PC, but the reticulated nature of the C–S–H gel can be clearly discerned in the microstructures of samples with a MgO to PC ratio of 1 to 1. An example of this is the region surrounding point "**B**" in Fig. 8c. In the same figure, the region near point "**C**" on the other hand is more consistent with $Mg(OH)_2$ or $Ca(OH)_2$ which both form with a similar habit. As the pfa content is lowered to 50 wt% as in Fig. 9, the volume taken up by the hydration products increasingly fills the space between the pfa particles and the hydration products become more intimately mixed. But the overall appearance is again one of a mixture of the products found in the samples where MgO and PC were not mixed.

To confirm the idea that the hydration processes of MgO and PC occur in parallel, the X-ray diffraction patterns of the mixed compositions $(MgO_{0.8}PC_{0.2})_{0.5}$–$pfa_{0.5}$ and $(MgO_{0.5}PC_{0.5})_{0.5}$–$pfa_{0.5}$ were calculated by linearly combining the diffraction patterns of the $MgO_{0.5}$–$pfa_{0.5}$ and $PC_{0.5}$–$pfa_{0.5}$ compositions, and superimposing them on the measured patterns in Fig. 5. Overall the agreement is good confirming that the two hydraulic components, i.e. PC and MgO, react independently of each other, very much analogous to the independent hydration behaviour of the phases in a cement clinker, which can also be assumed to hydrate independently [10,17].

The only real differences appear to be that Portlandite content is lower than expected and that the {1 0 1} peak of Brucite (2θ 37.98°) is slightly displaced to lower 2θ values and somewhat broadened. This could be evidence for some incorporation of Ca^{2+} into the Brucite structure. Indeed both Portlandite as well as Brucite have the same crystal structure but as the Ca^{2+} ion is larger than the Mg^{2+} ion this results in a larger spacing between the {1 0 1} planes in Portlandite than in Brucite. The increase in plane spacing as evidenced by the lowering of the 2θ angle of the diffraction peak, is in any case consistent with some Ca^{2+} incorporation into the Brucite.

4. Discussion

To determine whether the observed microstructures are consistent with what would be expected, the changes in solid volume that occur upon hydration need to be considered. For Portland cement this has been studied extensively and on average every gram of cement leads to the formation of 0.68 cm^3 of hydration products, including the porosity in the hydrated gel, which amounts to 0.18 cm^3 [10]. As discussed above when MgO hydrates, Brucite is the main hydration product and for the purposes of this calculation it is assumed to be the only hydration product. Brucite has a density of 2370 kg m^{-3} [10], and for every gram of MgO, 1.45 g of Brucite forms as is readily calculated from the stoichiometry of the reaction:

$$MgO + H_2O \rightarrow Mg(OH)_2 \quad (1)$$

Hence per gram of MgO, 0.61 cm^3 hydration product is formed, which is slightly lower than the volume of hydration product formed per gram of PC, consistent with the slightly larger coverage of the particles observed in the microstructures with a weight fraction pfa of 0.9, as was observed in Figs. 4 and 7. In terms of solid formed, the hydration of PC only gives 0.50 cm^3 per gram of PC, which is lower than the amount of solid formed due to the hydration of MgO. However, in terms of the observable filling of the gaps between the pfa particles, the PC gel will fill more space than the hydration of MgO. For the short time span considered in this study, it is assumed that the pfa remains unchanged.

To visualise the changes in volume and how the available space between the particles is filled, first the volume fraction of solids in the paste before hydration occurs is calculated assuming that the total volume is the sum of the volume of the solids and of the water. The resulting volume fractions of solid, $1 - P$, have been included in Table 2 and are quite close to the volume fraction of solid in a simple cubic stack of spheres, where every sphere of radius R_s is enclosed in a cube of edge length $2 \times R_s$, which is 0.524, suggesting that as an aid to understanding the microstructure such a simplified arrangement might indeed give some insight. To account for

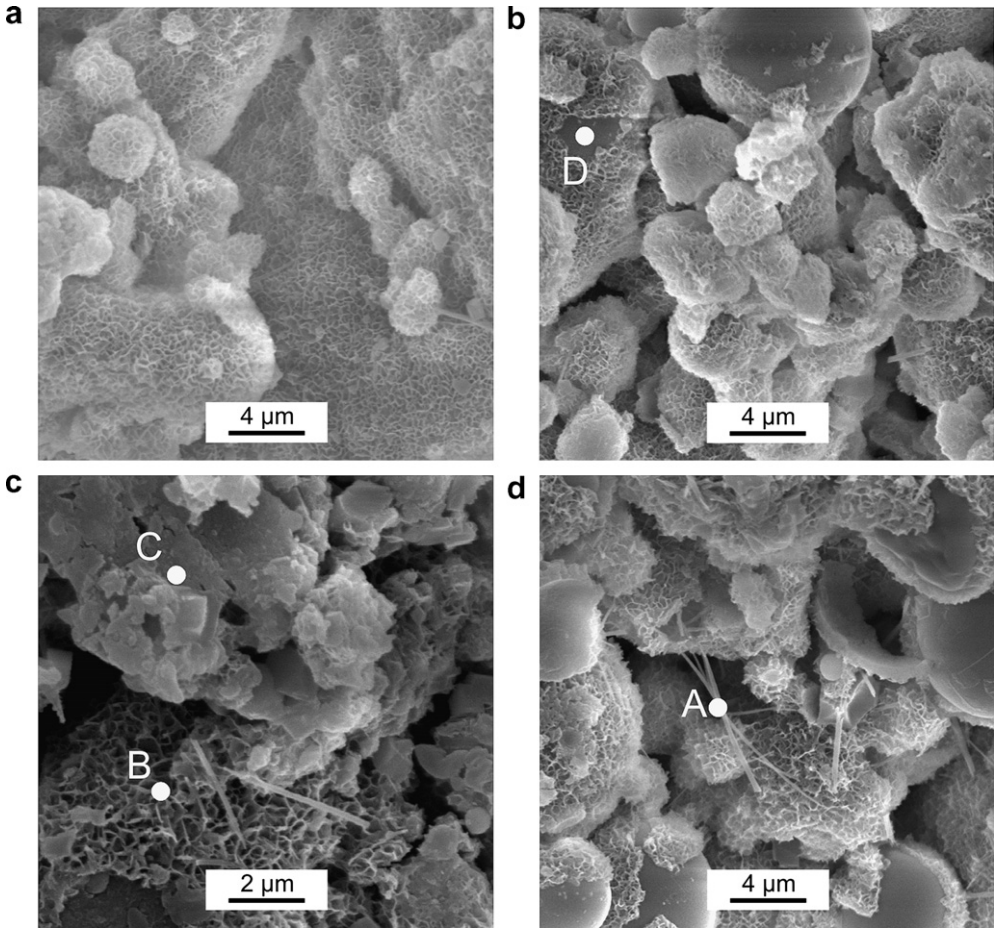

Fig. 8. Secondary electron micrographs after 14 days of hydration of samples with compositions (a-b) $(MgO_{0.8}PC_{0.2})_{0.1}$–$pfa_{0.9}$, (c–d) $(MgO_{0.5}PC_{0.5})_{0.1}$–$pfa_{0.9}$.

the differences in initial solid volume fractions, which tend to be slightly lower that 0.524 for mixtures with 50 wt% pfa, the radius of the sphere was adapted to give the calculated initial volume fraction of solids within a box with fixed size *a*. This is especially important for the compositions with high MgO content ($MgO_{0.5}$–$pfa_{0.5}$ and $(MgO_{0.5}PC_{0.5})_{0.5}$-$pfa_{0.5}$) as in order to form a paste for those blends, the water to solids ratio had to be increased.

Following on from this, the solid volume after hydration is calculated using the values estimated above, and this solid volume is deposited into the cube such that the solid becomes a sphere of radius R_d. If the overlap that develops is accounted for, the relation between the solid volume fraction and the ratio R_s and R_d is found to be:

$$(1-P) = \pi\left[\frac{3R_d^2}{4R_s^2} - \frac{R_d^3}{3R_s^3} - \frac{1}{4}\right] \quad (2)$$

Plotting the result as in Fig. 10 allows visualising the extent of bonding expected between the spheres. The calculation indicates that when a weight fraction pfa of 0.9 is used, there should only be a thin layer of hydration products covering the pfa particles, consistent with the observations. When the weight fraction pfa is reduced to 0.5, the calculation indicates that when PC is used extensive deposition and coverage of the pfa particles should occur as was observed, compare for example Fig. 10b with Fig. 7c, while for MgO the calculation indicates that the appearance still should be largely particulate in nature also consistent with observations as is clear from a comparison of Fig. 10a with Fig. 4c. The difference has two origins: the slightly lower space filling capacity of MgO relative to PC, but also the higher water to solids ratio that is needed for MgO. Hence, the higher water demand of the pastes with high MgO contents are a serious limitation to the density of material made with large amounts of reactive MgO.

One aspect that certainly contributes to the higher water demand is that the MgO particles tend to be finer as can be seen in Fig. 1, and fines tend to require more water. However, there is also a good case to be made for a fairly simple explanation. If it is assumed that the agglomerates that can be seen in Fig. 1a are not all broken up when the MgO powder is mixed with water, then these agglomerates act as porous particles. Since the size of these voids is much smaller than the size of the pfa or PC particles, these voids can only fill with water, thereby increasing the amount of water that is needed before the space between the all particles in the mix is filled and a paste is formed. Assuming the additional water needed to reach standard consistence, see Table 2, is indeed the water needed to fill the pores in the MgO agglomerates, then volume fraction of pores within the MgO agglomerates is estimated as 0.46 ± 0.07, which from the appearance of the agglomerates is certainly feasible. Another indication that actual chemical bonding might have occurred between particles in the MgO powder is the fact that it's bulk density quoted by the producer is 500 kg m^{-3} which is only 14% of the density of MgO. With the estimate for the internal porosity obtained above, this amounts to a packing efficiency of 26%. This figure compares favourably with loosely packed PC which has a bulk density of 1000 kg m^{-3} or a packing density of 31%. This suggests that if denser microstructures are desired, a slightly less reactive MgO powder, provided it does not show such extensive agglomeration

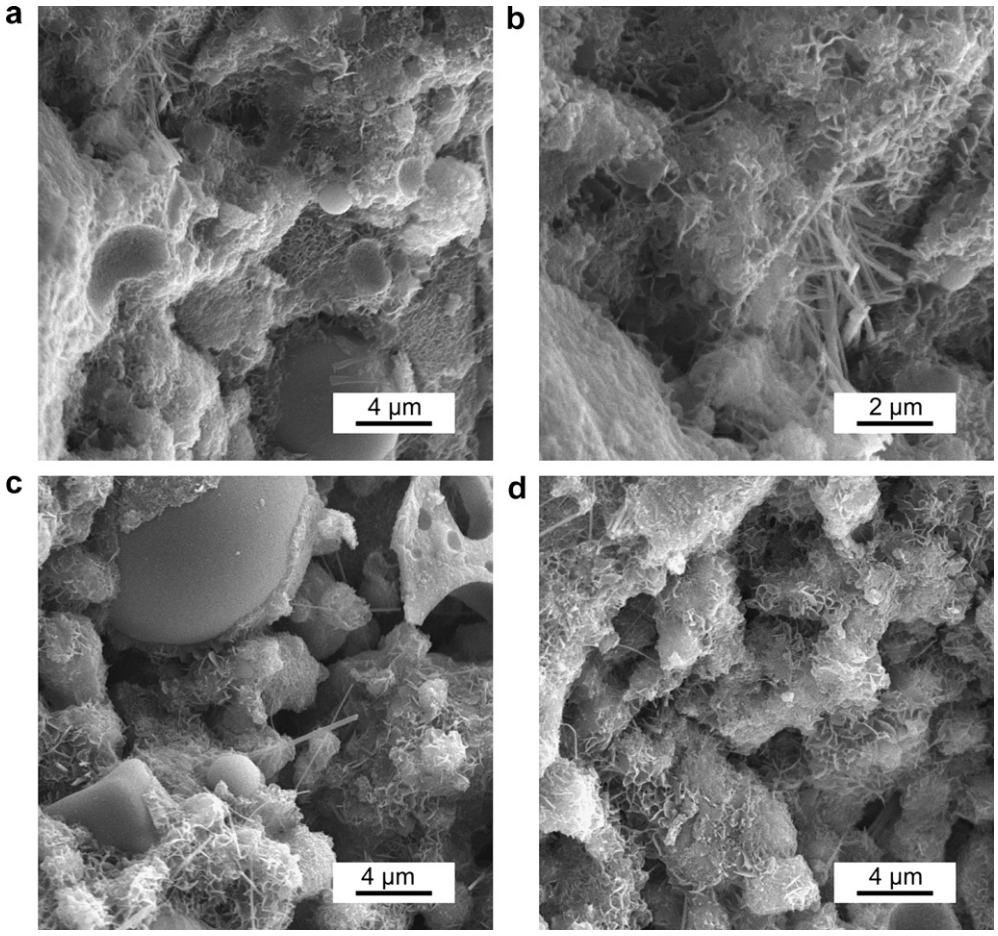

Fig. 9. Secondary electron micrographs after 14 days of hydration of samples with compositions (a–b) $(MgO_{0.8}PC_{0.2})_{0.5}$–$pfa_{0.5}$, (c–d) $(MgO_{0.5}PC_{0.5})_{0.5}$–$pfa_{0.5}$.

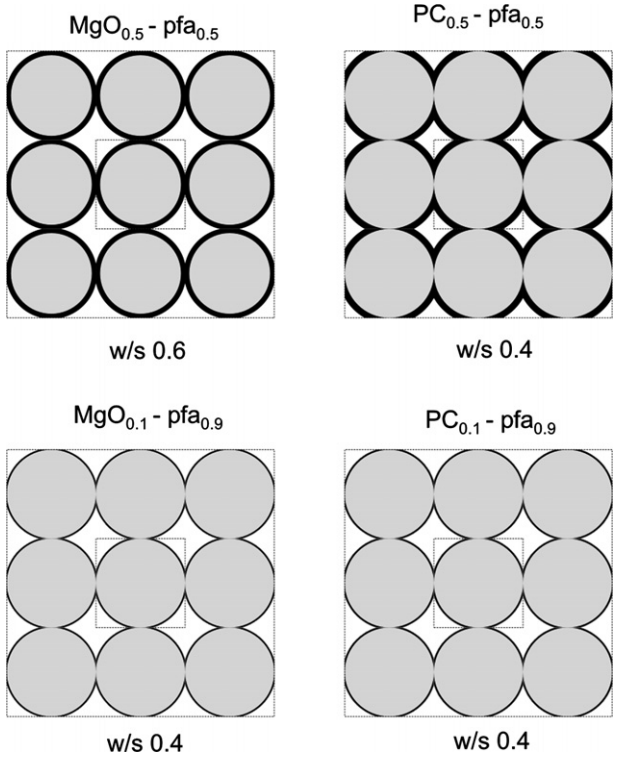

Fig. 10. schematic representation of calculated microstructures. The light grey sphere represents the volume fraction of solid before hydration, while black indicates the average volume fraction of solid after hydration.

and can still hydrate sufficiently in the correct time frame, could be advantageous.

5. Conclusions

The microstructures of blends of MgO, PC and pfa were studied as a function composition. At high pfa contents (weight fraction 0.9), the microstructure consists of pfa spheres onto which a thin coating of hydration products has formed, whereas when a lower amount of pfa is used (weight fraction 0.5) much more hydration product is formed and the coverage of the pfa particles becomes so extensive that the particulate nature of the microstructure starts to disappear. However, for mixes with very high MgO content ($MgO_{0.5}$–$pfa_{0.5}$ and $(MgO_{0.8}$–$PC_{0.2})_{0.5}$–$pfa_{0.5}$) the increased formation of hydration products is counteracted by the need to add more water to the pastes, which increases the volume that needs to be filled by hydration products. Brucite is the major hydration product due to MgO, with hydrotalcite as a minor component. After 64 days there is almost no unhydrated MgO left, so that there should be no risk for damage due to late hydration if a sufficiently reactive MgO is used. There was no evidence for a change in hydration products when MgO, PC and pfa are mixed compared to when either MgO and pfa or PC and pfa are mixed. The volume of hydration product per gram MgO of 0.61 $cm^3\,g^{-1}$, is slightly lower than the volume of hydration product formed per gram of PC of 0.68 $cm^3\,g^{-1}$, but higher than the amount of solid formed during hydration of PC of 0.50 $cm^3\,g^{-1}$. It is suggested that the higher water demand of the MgO powder is related to the presence of agglomerates, and estimates for the volume fraction of solids in the

agglomerates of 0.46 ± 0.07 are consistent with the very low bulk density of the MgO powder.

Acknowledgements

The work presented in this paper is part of an extensive research programme being carried out as part of a core Mini-Waste Faraday Partnership project entitled 'Waste minimisation through sustainable magnesium oxide cement products'. The project is led by Cambridge University and carried out in collaboration with Imperial College London and MIT and ten industrial collaborators including the inventor of the MgO cement technology John Harrison of TecEco Pty Ltd. The financial support provided by EPSRC, under grant GR/T26870/01, is gratefully acknowledged. The support from the Mini-Waste Faraday Partnership is also gratefully acknowledged.

References

[1] Harrison J. Reactive magnesium oxide cements. In: W.I.P. Organisation (Ed.), Australia; 2001.
[2] Ball MC. Reactions of compounds occurring in Sorel's cement. Cement Concrete Res 1977;7:575–84.
[3] Demediuk T, Cole WF, Hueber HV. Studies on magnesium and calcium oxychlorides. Aust J Chem 1955;8:215–33.
[4] Cole WF, Demediuk T. X-ray, thermal, and dehydration studies on magnesium oxychlorides. Aust J Chem 1955;8:235–51.
[5] Hewlett PC, editor. Lea's chemistry of cement and concrete. London: Arnold; 1998. p. 1053.
[6] Soudee E, Pera J. Mechanism of setting reaction in magnesia-phosphate cements. Cement Concrete Res 2000;30(2):315–21.
[7] Soudee E, Pera J. Influence of magnesia surface on the setting time of magnesia-phosphate cements. Cement Concrete Res 2002;32(1):153–7.
[8] BSI, Methods of testing cement. Determination of setting time and soundness, British Standards; 1994.
[9] Wesche K, editor. Fly ash in concrete: properties and performance* RILEM Report 7. London: Chapman and Hall; 1991. p. 255.
[10] Mindess S, Young JF, Darwin D. Concrete. 2nd ed.. Prentice Hall: Upper Saddle River; 2003. p. 644.
[11] Ahari KG, Sharp JH, Lee WE. Hydration of refractory oxides in castable bond systems-I: alumina, magnesia, and alumina–magnesia mixtures. J Eur Ceram Soc 2002;22(4):495–503.
[12] Ahari KG, Sharp JH, Lee WE. Hydration of refractory oxides in castable bond systems – II: alumina–silica and magnesia–silica mixtures. J Eur Ceram Soc 2003;23(16):3071–7.
[13] Brew DRM, Glasser FP. Synthesis and characterisation of magnesium silicate hydrate gels. Cement Concrete Res 2005;35:85–98.
[14] Cole WF. A crystalline hydrated magnesium silicate formed in the breakdown of a concrete sea-wall. Nature 1953;171:354–5.
[15] Bonen D, Cohen MD. Magnesium sulfate attack on Portland cement paste – II. Chemical and mineralogical analyses. Cement Concrete Res 1992;22:707–18.
[16] Jennings HM. A model for the microstructure of calcium silicate hydrate in cement paste. Cement Concrete Res 2000;30(1):101–16.
[17] Tennis PD, Jennings HM. A model for two types of calcium silicate hydrate in the microstructure of Portland cement pastes. Cement Concrete Res 2000;30(6):855–63.
[18] Constantinides G, Ulm FJ. The effect of two types of C–S–H on the elasticity of cement-based materials: results from nanoindentation and micromechanical testing. Cement Concrete Res 2004;34(1):67–80.
[19] Song S, Jennings HM. Pore solution chemistry of alkali-activated ground granulated blast-furnace slag. Cement Concrete Res 1999;29:159–70.